AGU100 ADVANCING EARTH AND SPACE SCIENCE

Geophysical Research Letters

Key Points:
- Observed excess heat (Q') and anthropogenic carbon storage in the Southern Ocean shows contrasting spatial patterns
- Eddy-resolving model reveals that circulation change controls Q' storage; carbon storage anomaly (C') behaves more like a passive tracer
- A responsive surface buoyancy flux results in a greater sensitivity of net circulation change in response to wind stress change

Supporting Information:
- Supporting Information S1

Correspondence to:
H. Chen,
haidic@princeton.edu

Deciphering Patterns and Drivers of Heat and Carbon Storage in the Southern Ocean

Haidi Chen[1] (iD), **Adele K. Morrison[2]** (iD), **Carolina O. Dufour[3]** (iD), and **Jorge L. Sarmiento[1]** (iD)

[1]Atmospheric and Oceanic Sciences, Princeton University, Princeton, NJ, USA, [2]Research School of Earth Sciences and ARC Centre of Excellence for Climate Extremes, Australian National University, Canberra, ACT, Australia, [3]Department of Atmospheric and Oceanic Sciences, McGill University, Montreal, Quebec, Canada

Abstract The storage of anomalous heat and carbon in the Southern Ocean in response to increasing greenhouse gases greatly mitigates atmospheric warming and exerts a large impact on the marine ecosystem. However, the mechanisms driving the ocean storage patterns are uncertain. Here using recent hydrographic observations, we compare for the first time the spatial patterns of heat and carbon storage, which show substantial differences in the Southern Ocean, in contrast with the conventional view of simple passive subduction into the thermocline. Using an eddy-rich global climate model, we demonstrate that redistribution of the preindustrial temperature field is the dominant control on the heat storage pattern, whereas carbon storage largely results from passive transport of anthropogenic carbon uptake at the surface. Lastly, this study highlights the importance of realistic representation of wind and surface buoyancy flux in climate models to improve future projection of circulation change and thus heat and carbon storage.

1. Introduction

The Southern Ocean (SO), south of 30°S, is estimated to account for 75 ± 22% of the global oceanic uptake of excess heat and 30–40% of the global oceanic uptake of excess carbon from the atmosphere (Frölicher et al., 2015; Khatiwala et al., 2009). The subsequent storage of the excess heat (Q') and carbon (C') in the SO can further feedback on oceanic heat uptake and carbon buffering capacity (Egleston et al., 2010; Riebesell et al., 2009) and exert significant impact on large-scale marine ecosystems (Nagelkerken & Connell, 2015; Wohlers et al., 2009). Here excess heat and carbon refer respectively to the net change in temperature and dissolved inorganic carbon (DIC) in the ocean, resulting from the additional surface flux and interior redistribution of the preindustrial temperature and DIC. An improved understanding of the spatial variability of Q' and C' storage in the SO and their underlying mechanisms is essential to provide the baseline for future assessments of oceanic heat and carbon sequestration, and to understand the feedbacks on global climate.

The two dominant mechanisms that have been proposed are passive and redistributive tracer transport convergence (e.g., Banks & Gregory, 2006; Winton et al., 2013). Passive transport corresponds to the transport of anomalous (anthropogenic) heat and carbon taken up at the ocean surface and advected into the interior by the ocean circulation. Thus, Q' and C' storage driven by passive transport reflect the storage of anthropogenic heat (H_{ant}) and carbon (C_{ant}). Large-scale studies that have focused separately on either heat (Armour et al., 2016; Church et al., 1991; Jackett et al., 2000) or carbon (Iudicone et al., 2016; Khatiwala et al., 2013; Sabine et al., 2004), have suggested that passive transport is the primary driver of Q' and C' storage in the SO. However, this perspective is questioned by several model-based studies that have proposed that the redistributive transport, which refers to a redistribution of the preindustrial tracer fields by the anomalous circulation, can have a comparable impact in shaping spatial patterns of Q' (Frölicher et al., 2015; Winton et al., 2013). The importance of circulation change for C' storage is still an open question (DeVries et al., 2017; Winton et al., 2013).

Fundamental to solving the question of whether the passive or redistributive transport dominates is to know the extent to which the net circulation has changed over time. The total transport is composed of the Eulerian mean (zonal and temporal mean) and eddy transport (including transient and stationary eddies; Marshall & Speer, 2012). While the Eulerian mean transport can be estimated from the wind, the eddy transport is difficult to quantify from observations and is not explicitly resolved in most current Earth system models. Accurately determining the change in the eddy transport, and therefore the net circulation

change, is challenging, making it difficult to disentangle the influence of passive and redistributive transport in shaping the Q' and C' storage patterns in the SO.

In this paper we aim to address the following questions: What are the storage patterns of Q' and C' in the SO interior? What are the relative contributions of the passive and redistributive transports in setting their storage patterns? To answer these questions, we use recent observational-based data sets to determine the storage patterns, and a state-of-the-art, eddy-rich global climate model to investigate the underlying processes that regulate the storage patterns.

2. Materials and Methods

2.1. Observational-Based Reconstructions

The ocean heat content (OHC) is calculated using objectively analyzed monthly mean potential temperature data from the Met Office Hadley Centre's EN4 version 2.0 (Good et al., 2013; https://www.metoffice.gov.uk/hadobs/en4/). Due to sparse sampling and the resulting large OHC error in the early era, the Q' storage is calculated as the OHC difference between the 10-year mean periods 2002–2011 and 1972–1981. Because DIC measurement in the SO before 1990 is extremely limited, C' storage cannot be accurately quantified. However, C_{ant} storage, the passive component of C', has been constructed using the Greens function method that is accurate to $\pm 2\%$ (Khatiwala et al., 2009). Here we use C_{ant} storage provided by Khatiwala et al. (2009, 2013) and calculate the C_{ant} accumulation using the 10-year periods of 1972–1981 to 2002–2011.

2.2. Model

We use the eddy-resolving Geophysical Fluid Dynamics Laboratory (GFDL) CM2.6 global climate model (Delworth et al., 2012; Griffies et al., 2015), coupled to the biogeochemical model miniBLING (Galbraith et al., 2015), to analyze the mechanisms driving Q' and C' storage in the SO (Supporting Information Text S1). CM2.6 consists of a 0.1° resolution ocean model, a 50-km resolution atmospheric model, and sea ice and land models. The Q' and C' storage in CM2.6 is defined as the difference between a control simulation forced with preindustrial atmospheric CO_2 (CO_2^{atm}) and a climate change simulation forced with CO_2^{atm} increasing at a rate of 1% per year run following 120 years of the preindustrial simulation. The diagnostics for the C' budget are not saved before CO_2^{atm} reaches 524 ppm; therefore, we evaluate a 10-year average period just preceding CO_2^{atm} doubling (years 60–70 of the climate simulation), for which 5-day average model output was saved. We refer the reader to Griffies et al. (2015), Dufour et al. (2015), and Morrison et al. (2016) for an in-depth description of the SO state in CM2.6.

3. Results

3.1. Heat and Carbon Storage Patterns

The observationally reconstructed SO Q' and C_{ant} storage differ significantly in their latitudinal and vertical distributions (Figures 1a and 1b). The Q' storage shows strong spatial heterogeneity, with a significant fraction of Q' stored between 38° and 50°S, penetrating from the surface down to 1,200-m depth. North of 38°S, a nonnegligible amount of Q' is also stored in the top 300-m but minimal or even reduced Q' storage is observed below 300-m (Figure 1a). The C_{ant} storage peaks at the sea surface north of 38°S and decreases smoothly southward and downward (Figure 1b). To our knowledge, this work compares for the first time these two observed storage patterns. As C_{ant} storage does not include changes in the preindustrial carbon cycle, the difference between the Q' and C_{ant} storage patterns suggests that redistributive transport is not negligible. The distribution of Q' and C' storage simulated by CM2.6 is very similar to the Q' and C_{ant} constructed from observations (Figures 1c and 1d), although the model's storage is about 3 times larger due to a longer accumulation time of the anthropogenic signal. Due to the pattern similarity between observed C_{ant} and simulated C', we infer that either the impact of redistributive transport on C' storage is small or it reinforces the passive transport.

3.2. Physical Processes Driving Q' and C' Storage

We use CM2.6 to quantify the dominant processes responsible for setting the spatial patterns of Q' and C' storage. Q' and C' storage results from the respective time-integrated tendency difference between climate and preindustrial simulations calculated over a 70-year period. Beneath the surface layer, the Q' and C'
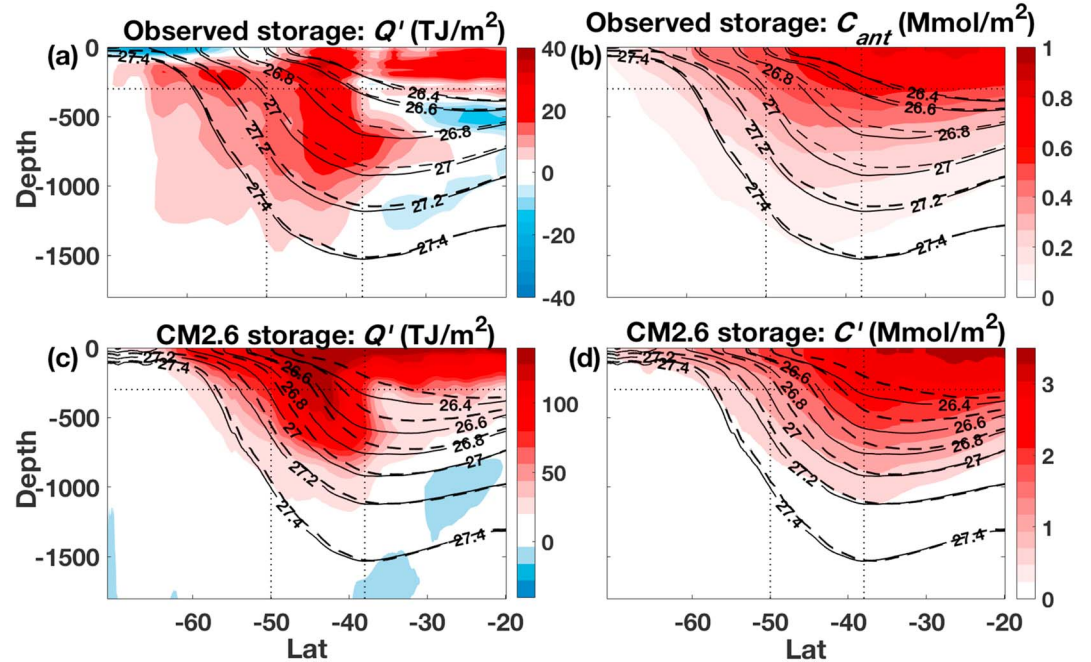
Figure 1. Zonally integrated excess heat (Q') and carbon (C') storage. Observation-based reconstruction of (a) Q' and (b) anthropogenic carbon (C_{ant}) storage. Simulated CM2.6 storage of (c) Q' and (d) C'. Black contours in (a) and (b) show the zonal mean potential density (σ_0) from EN4 data averaged between 1972 and 1981 (dashed) and between 2002 and 2011 (solid). Black contours in (c) and (d) are CM2.6 σ_0 from preindustrial (dashed) and climate (solid) simulations. Dotted vertical lines mark latitudes 50° and 38°S, and horizontal lines mark 300-m depth.

storage tendencies are impacted by transport convergence (advection), parameterized submesoscale processes, and vertical mixing (Text S1). While the available model output only allows us to calculate the tendency terms over a 10-year period, the 10-year mean Q' and C' tendencies in the interior ocean (Figures 2a and 2b) have a similar pattern to the 70-year storage (Figures 1c and 1d). In the model, below the winter maximum mixed-layer depth (MLD_{max}), transport convergence controls the storage patterns, and explains the difference between Q' and C' across the intermediate (38–50°S) and the northern (north of 38°S) regions (Figures 2c and 2d). Submesoscale processes, vertical mixing, and biology are only significant within the mixed layer (Figure S1). In this study, we only focus on the storage patterns and processes in the interior ocean below the MLD_{max}.

Next, we examine the total tracer transport convergence (Figures 2c and 2d) separated into its passive and redistributive components. In the climate simulation, a velocity v that advects a tracer χ, either heat or carbon, can be written as

$$v = v_{1860} + \Delta v; \chi = \chi_{1860} + \Delta \chi, \tag{1}$$

where subscript 1860 refers to the variables in the preindustrial simulation. Δ indicates the difference between the climate and preindustrial simulations. The change in total tracer transport convergence in response to CO_2 increase can be decomposed into two components:

$$\nabla \cdot (v\chi) - \nabla \cdot (v_{1860} \chi_{1860}) = \nabla \cdot (\chi_{1860} \Delta v) + \nabla \cdot (v\Delta \chi). \tag{2}$$

The right-hand side of equation (2) represents the change associated with the direct impact from circulation change (first term) and the change associated with the tracer anomaly (second term). Following Garuba and Klinger (2016), we use *redistributive transport* to refer to $\chi_{1860}\Delta v$, and *passive transport* to refer to $v\Delta\chi$. Equation (2) allows a qualitative analysis of the passive and redistributive components of the tracer storage. Unfortunately, this analysis is limited to being qualitative only, because we are unable to isolate the effect of the redistribution feeding back onto the surface uptake (Text S2). Specifically, a stronger imprint of the first term on the total transport convergence would suggest that the circulation change plays the dominant role in
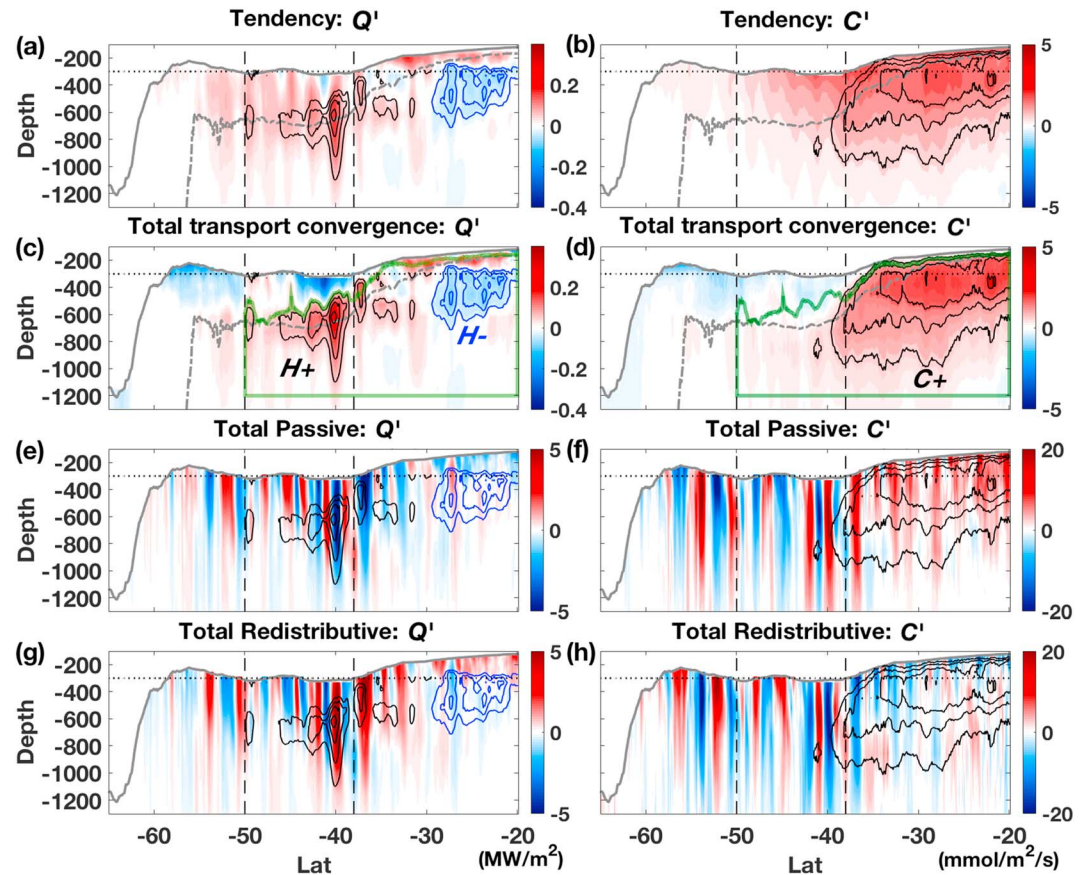
Figure 2. Zonally integrated storage tendencies for Q' (left) and C' (right). Total storage tendencies (a, b) are compared with the total transport convergences (c, d), which are decomposed into total passive (e, f) and redistributive (g, h) components. Gray solid and dashed lines are zonal mean MLD_{max} and zonal maximum MLD_{max}, respectively. To highlight the processes below the mixed layer, values within the MLD_{max} are masked out but shown in Figure S1. Black and blue contours in (c) and (d) highlight the locations where large positive and negative transport convergences are found below the MLD_{max}; these contours are overlaid on (a)–(h). The closed green line in (c) and (d) defines the region where tracer correlation analysis is performed (Figure 3) and is composed within the peak Q' storage region at 38–50°S (noted as $H+$ region) and the peak C' storage region at 20–38°S (noted as $C+$ region). Within the $C+$ region, a minimum Q' storage is found, and we use $H-$ to refer to the region covered by blue contours in (c).

tracer storage. Alternatively, the dominance of passive transport would result in a closer approximation of the second term to the total transport convergence. The transport components are calculated using 5-day averaged output, and the sum of the redistributive and passive components is consistent with the total advection anomaly (calculated online).

We apply the decomposition from equation (2) to investigate the Q' and C' storage patterns (Figures 2e–2h). Where Q' storage is maximum or minimum, we find significant positive correlation between the total transport convergence of Q' and that of total redistributive transport ($r = 0.54$, $p < 1e^{-24}$; Figure 2g). In contrast, Q' storage peaks are generally collocated with the divergence of total passive transport (Figure 2e). Therefore, we conclude that redistributive transport controls the Q' storage. For C', the total passive transport shows strong convergence to the north of 38°S and is collocated with the C' storage maxima below the MLD_{max} (Figure 2f), whereas total redistributive transport shows weak divergence (Figure 2h). Therefore, passive transport plays a dominant role in C' storage. The dominance of passive transport in C' storage also explains why there is strong pattern similarity between C' storage and the observationally reconstructed C_{ant} storage. Further inspection also shows that the passive and redistributive terms are anticorrelated and of similar magnitude, resulting in a smaller magnitude of their sum. While we do not have a complete understanding of the cause of the large cancellation between the passive and redistributive terms, we note that it is dominated by the eddy component and hypothesize that it is related to shifting fronts and jets in the SO.

Because the total transport is the residual between the Eulerian mean and eddy transports, we next look into the degree of eddy compensation relative to the Eulerian mean (Text S3). The peak Q' storage at 38–50°S, averaged between the MLD_{max} and 1,200-m results from a strong convergence driven by the Eulerian mean transport (0.12 MW/m^2), partially offset by eddy divergence (−0.07 MW/m^2). Similarly, the peak C' storage to the north of 38°S (0.9 mmol/m^2/s) is primarily controlled by the Eulerian mean convergence (1.0 mmol/m^2/s). Thus, in the regions of peak Q' and C' storage, eddy compensation is incomplete. We also find that the passive and redistributive components of the Eulerian mean transport convergence play qualitatively similar roles as in the total transport convergence: Eulerian mean Q' convergence at 38–50°S is mainly controlled by redistributive transport, and Eulerian mean C' convergence to the north is mainly controlled by passive transport (Figure S2).

3.3. Quantitative Contribution

Here we provide a quantitative estimate of the redistributive and passive components of the tracer convergence by performing a regression analysis with phosphate convergence. Phosphate is a tracer that is redistributed by the changing circulation in a similar way to heat and carbon but is not directly affected by air-sea flux changes. We first demonstrate that there is a strong heat-carbon-phosphate transport coupling in the control simulation by examining the relationship between the transport tendency of phosphate (P) and the transport tendencies of heat or carbon (χ) according to

$$\nabla\cdot(\widehat{\chi_{1860}v_{1860}}) = a_1\nabla\cdot(P_{1860}v_{1860}) + a_2\,J^P_{1860} + a_3, \tag{3}$$

where $[a_1, a_2, a_3]$ are regression coefficients for heat or carbon transport convergence and ^ represents the predicted advection. The biological sink and source for phosphate, J^P, is included to separate the biological driven variability of phosphate from the physically based circulation effect. We use a least squares fit to equation (3) and find that more than 80% of the spatial variance in heat and carbon transport convergence can be explained by phosphate convergence in the control run (Figures 3a and 3b). These relationships are then applied to the transport tendency of phosphate in the climate simulation to estimate what the patterns of Q' and C' would be if they were only impacted by circulation change. The difference between the empirical predictions and the transport tendencies in the climate simulation can be considered as largely reflecting the impact from passive transport (Text S4).

Our empirical analysis supports our qualitative evaluation of the relative importance of passive and redistributive transport (Figure 3c). At 38–50°S, we estimate that redistributive transport contributes $60 \pm 4\%$ of the Q' storage ("$\pm$" is the 95% confidence interval for the regression coefficients) between the MLD_{max} and 1,200-m (Figure 3c). By contrast, only $21 \pm 1\%$ of the peak C' storage to the north of 38°S (Figure 3c) is attributed to the redistributive transport. For regions where Q' (north of 38°S) and C' storage (38–50°S) tendencies are low, opposing tendencies are found between passive and redistributive transports. Our quantification is subject to the uncertainty related to the influence of biological processes (see equation (3) and Text S4). We quantify this uncertainty by comparing to an extreme case using only the transport tendency of phosphate in equation (3). We find that excluding J^P in equation (3) increases the contribution of redistributive transport to Q' storage by 3% in the intermediate region and to C' storage by 7% in the northern region. Therefore, the uncertainty related to the biological influence on phosphate is small.

4. Discussion

4.1. Drivers of Circulation Change

Since the storage pattern difference between Q' and C' arises from circulation change, we further explore the forcing that drives the changes in the SO residual meridional overturning circulation (Ψ_{res}). The SO Ψ_{res} is dominated by deep water rising towards the surface within the Antarctic Circumpolar Current (ACC), which splits into upper and lower overturning circulation cells by flowing either northward or southward near the surface (Marshall & Speer, 2012). The surface meridional transport crosses isopycnals in the surface diabatic layer, balanced with the surface buoyancy flux B (Marshall & Radko, 2003).

We calculate Ψ_{res} in isopycnal coordinates and map to depth coordinates by using the mean depth of isopycnal surfaces (Figure S4). In the climate simulation, enhanced surface buoyancy gain occurs due to a warmer
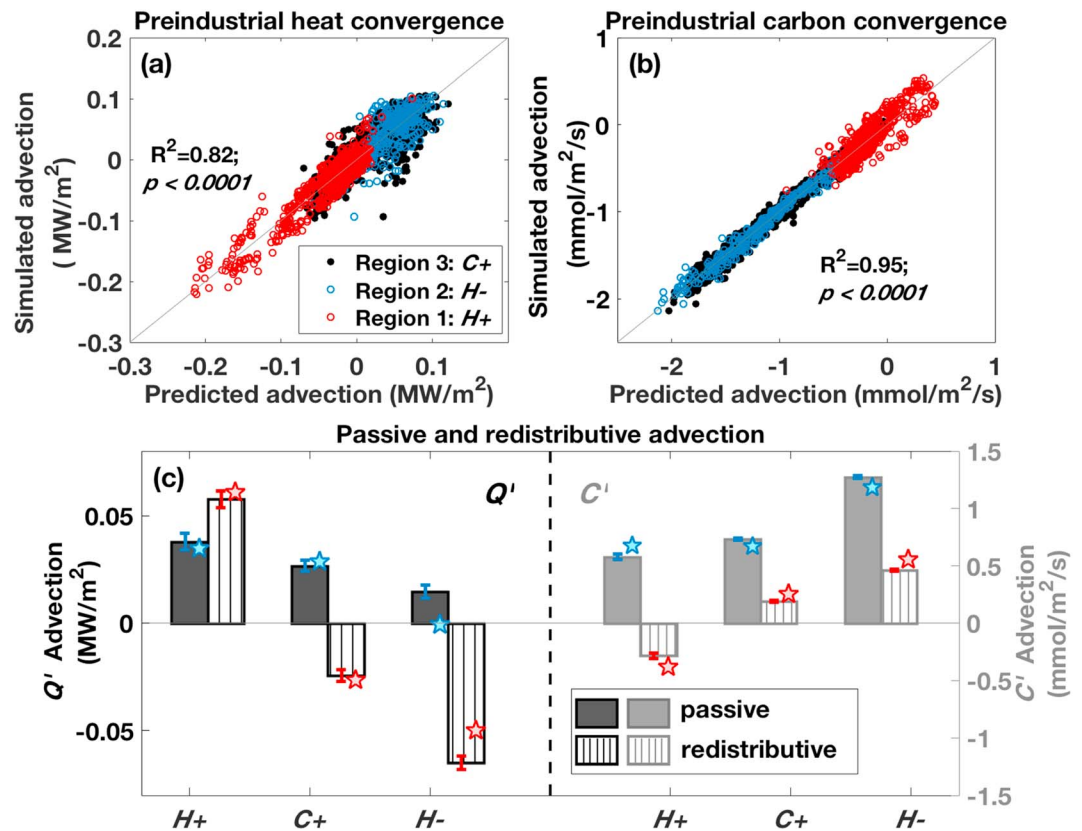
Figure 3. Quantitative analysis of the Q' and C' storage driven by passive and redistributive advection in the three regions defined in Figure 2c (also Figure S3). CM2.6 advection of (a) heat and (b) carbon in the preindustrial simulation versus the empirically predicted advection computed from regression fittings (equation (3)). (c) Area-averaged passive (filled bars) and redistributive (hatched bars) advection for Q' (black, left y axis) and C' storage (gray; right y axis) predicted from the empirical relationships for the three regions. Error bars represent the 95% confidence interval for the regression coefficients. Predictions using the transport convergence of phosphate as the only regressor are compared and shown as blue (passive storage) and red (redistributive storage) stars.

atmosphere driving a larger amount of heat flux into the ocean (Figure 4). Between 45° and 55°S, a positive buoyancy gain anomaly ($\Delta B > 0$) on outcropping isopycnals lightens the dense upwelled water compared with the control simulation, and an increased northward volume transport ($\Delta\Psi_{\mathrm{res}} > 0$) in the upper ocean is required to satisfy the buoyancy budget. Further north, anomalous buoyancy gain occurs at 35–40°S over the southward subduction limb of the shallow subtropical cell, and a large decrease in the southward transport at the surface is also required ($\Delta\Psi_{\mathrm{res}} > 0$). Between these two regions of large anomalous buoyancy gain, there is a unique region around 40–45°S with buoyancy loss ($\Delta B < 0$). The lack of anomalous heat flux into the ocean between 40° and 45°S cannot be explained by the atmospheric warming pattern, which is nearly uniform across these latitudes. Rather, this region coincides with the depth-integrated Q' storage maxima, which reduces the air-sea temperature difference and provides a negative feedback on the heat flux, as suggested in previous model studies (Armour et al., 2016; Garuba & Klinger, 2016, 2018). The northward transport between 40° and 45°S weakens in the climate simulation ($\Delta\Psi_{\mathrm{res}} > 0$), consistent with the negative buoyancy flux anomaly. The changes in the upper ocean meridional transport described above drive regions of surface convergence (42–50°S) and divergence (35–42°S), as shown in Figure 4. As a result, a downward and an upward transport anomaly occurs in the intermediate and the northern regions, respectively.

The change in surface buoyancy flux also results in a greater sensitivity of Ψ_{res} to wind stress changes near the ACC (Abernathey et al., 2011; Morrison et al., 2011; Figures 4 and S5). To the south of 45°S, the northward transport of Ψ_{res} at the surface increases as a result of increasing zonal wind stress, in conjunction with incomplete eddy compensation (Morrison & Hogg, 2013). Between 40° and 45°S, the reduced northward
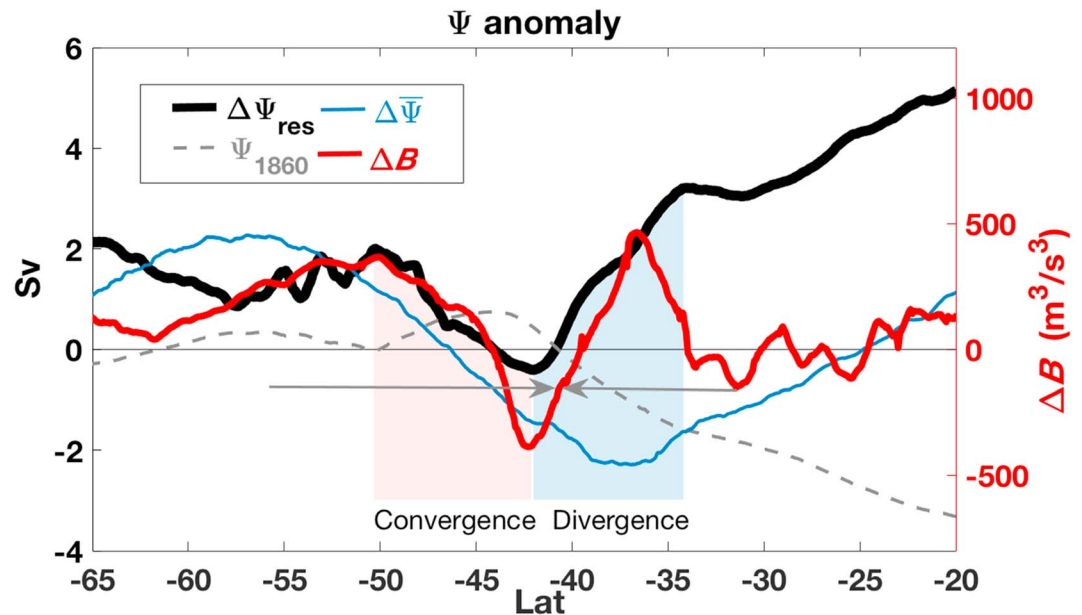
Figure 4. Residual mean meridional overturning circulation in the control simulation (Ψ_{1860}, scaled by 0.1) and the change in the climate simulation ($\Delta\Psi_{res}$), averaged in the upper 100-m. The change in the Eulerian mean circulation ($\Delta\overline{\Psi}$) is shown by the blue line. Zonally integrated surface buoyancy flux anomaly (ΔB) is plotted against the right y axis (red). The red and blue shading highlight the latitudinal regions where $\Delta\Psi_{res}$ has strong convergence and divergence in the surface layer. The two gray arrows indicate the northward or southward transport of Ψ_{1860} at the surface.

transport also coincides with the reduction of the wind stress to the north of 45°S (Figure S6). Further north of 40°S, the decreased southward transport by the subtropical cell is controlled by the change in the eddy circulation at the surface (Ψ'), as the change in the wind-driven mean circulation opposes the change in the residual circulation. The large decrease in the magnitude of Ψ' is consistent with the significant flattening of the isopycnal slopes in the upper 300 m north of 40°S in the climate simulation.

4.2. Relative Importance of Redistributive Transport

Since temperature and carbon have opposite spatial gradients, the net circulation anomaly can result in a large storage contrast between Q' and C'. However, difference in storage patterns also depends on the magnitude of the redistributive transport relative to the passive transport (Winton et al., 2013). From 1972–1981 to 2002–2011, the SO has warmed by 0.2–0.3 °C to the north of ACC (from observation-based reconstructions). Such warming intensity, however, is much smaller than the preindustrial vertical temperature difference, which is on the order of 10 °C difference from the surface to the deep ocean (e.g., 1 km). Therefore, a spatial redistribution of the existing temperature field could easily overwhelm the impact of passive transport of anthropogenic heat. In contrast, surface C_{ant} concentration in the SO has increased by 20–30 µmol/kg from 1972–1981 to 2002–2011, still smaller than but more comparable with the vertical difference in preindustrial carbon (on the order of 200 µmol/kg difference from the surface to the deep ocean). The model simulated changes are scaled consistently with the observations, although the model shows larger magnitude changes (surface temperature and carbon increase respectively on the order of 1 °C and 100 µmol/kg over the 70-year climate run). Therefore, both model and observations suggest that passive transport exerts a larger impact on C' storage than on Q' storage, and C_{ant} storage is a close approximation of C' storage. Under continued CO_2 forcing in the future, passive transport could dominate the storage pattern for both Q' and C'.

5. Conclusion

Our study based on recent observations and a high-resolution climate model highlights two main results: Q' and C' storages differ significantly in their spatial patterns in the SO; and the circulation change is an essential component in driving their spatial dissimilarity. These findings have two important implications. First, knowing the patterns of Q' and C' is crucial for accurately modeling seawater chemistry. Changes in oceanic

seawater chemistry, including ongoing ocean acidification (Doney et al., 2009), critically depend on spatial patterns of Q' and C' storage, which largely regulate the CO_2 buffering capacity, and can alter marine ecosystems (Doney et al., 2012; Poloczanska et al., 2013). Our advanced understanding here can thus improve the projection of future carbon uptake and marine ecosystem functioning (Falkowski et al., 1998). Second, the predominance of passive transport on C' storage further suggests that relatively coarser-resolution models would be able to reproduce the C' storage, with an acceptable representation of the mean state of the ocean circulation. Low-resolution models do generate a pattern contrast between Q' and C' storage (Frölicher et al., 2015). However, to correctly simulate the Q' storage, an accurate representation of the mean and eddy circulation is needed. Oceanic circulation changes remain one of the most challenging components to accurately simulate. Since changes in ocean circulation are mainly responsible for the large variability between models in ocean Q' uptake and storage (Frölicher et al., 2015; Kostov et al., 2014), improved understanding of the fundamental drivers of future oceanic circulation is critically needed.

References

Abernathey, R., Marshall, J., & Ferreira, D. (2011). Dependence of Southern Ocean overturning on wind stress. *Journal of Physical Oceanography*, 41(12), 2261–2278. https://doi.org/10.1175/JPO-D-11-023.1

Armour, K. C., Marshall, J., Scott, J. R., Donohoe, A., & Newsom, E. R. (2016). Southern Ocean warming delayed by circumpolar upwelling and equatorward transport. *Nature Geoscience*, 9(7), 549–554. https://doi.org/10.1038/ngeo2731

Banks, H. T., & Gregory, J. M. (2006). Mechanisms of ocean heat uptake in a coupled climate model and the implications for tracer based predictions of ocean heat uptake. *Geophysical Research Letters*, 33, L07608. https://doi.org/10.1029/2005GL025352

Church, J. A., Godfrey, J. S., Jackett, D. R., & McDougall, T. J. (1991). A model of sea-level rise caused by ocean thermal expansion. *Journal of Climate*, 4(4), 438–456. https://doi.org/10.1175/1520-0442(1991)004<0438:AMOSLR>2.0.CO;2

Delworth, T. L., Rosati, A., Anderson, W., Adcroft, A. J., Balaji, V., Benson, R., et al. (2012). Simulated climate and climate change in the GFDL CM25 high-resolution coupled climate model. *Journal of Climate*, 25(8), 2755–2781. https://doi.org/10.1175/JCLI-D-11-00316.1

DeVries, T., Holzer, M., & Primeau, F. (2017). Recent increase in oceanic carbon uptake driven by weaker upper-ocean overturning. *Nature*, 542(7640), 215–218. https://doi.org/10.1038/nature21068

Doney, S. C., Fabry, V. J., Feely, R. A., & Kleypas, J. A. (2009). Ocean acidification: The other CO_2 problem. *Annual Review of Marine Science*, 1(1), 169–192. https://doi.org/10.1146/annurev.marine.010908.163834

Doney, S. C., Ruckelshaus, M., Duffy, J. E., Barry, J. P., Chan, F., English, C., et al. (2012). Climate change impacts on marine ecosystems. *Annual Review of Marine Science*, 4(1), 11–37. https://doi.org/10.1146/annurev-marine-041911-111611

Dufour, C. O., Griffies, S. M., De Souza, G. F., Frenger, I., Morrison, A. K., Palter, J. B., et al. (2015). Role of mesoscale eddies in cross-frontal transport of heat and biogeochemical tracers in the Southern Ocean. *Journal of Physical Oceanography*, 45(12), 3057–3081. https://doi.org/10.1175/JPO-D-14-0240.1

Egleston, E. S., Sabine, C. L., & Morel, F. M. M. (2010). Revelle revisited: Buffer factors that quantify the response of ocean chemistry to changes in DIC and alkalinity. *Global Biogeochem Cycles*, 24, GB1002. https://doi.org/10.1029/2008GB003407

Falkowski, P. G., Barber, R. T., & Smetacek, V. (1998). Biogeochemical controls and feedbacks on ocean primary production. *Science*, 281(5374), 200–206. https://doi.org/10.1126/science.281.5374.200

Frölicher, T. L., Sarmiento, J. L., Paynter, D. J., Dunne, J. P., Krasting, J. P., & Winton, M. (2015). Dominance of the Southern Ocean in anthropogenic carbon and heat uptake in CMIP5 models. *Journal of Climate*, 28(2), 862–886. https://doi.org/10.1175/JCLI-D-14-00117.1

Galbraith, E. D., Dunne, J. P., Gnanadesikan, A., Slater, R. D., Sarmiento, J. L., Dufour, C. O., et al. (2015). Complex functionality with minimal computation: Promise and pitfalls of reduced-tracer ocean biogeochemistry models. *Journal of Advances in Modeling Earth Systems*, 7, 2012–2028. https://doi.org/10.1002/2015MS000463

Garuba, O. A., & Klinger, B. (2016). Ocean heat uptake and interbasin transport of the passive and redistributive components of surface heating. *Journal of Climate*, 29(20), 7507–7527. https://doi.org/10.1175/JCLI-D-16-0138.1

Garuba, O. A., & Klinger, B. (2018). The role of individual surface flux component in the passive and active ocean heat uptake. *Journal of Climate*, 31(15), 6157–6173. https://doi.org/10.1175/JCLI-D-17-0452.1

Good, S. A., Martin, M. J., & Rayner, N. A. (2013). EN4: Quality controlled ocean temperature and salinity profiles and monthly objective analyses with uncertainty estimates. *Journal of Geophysical Research: Oceans*, 118, 6704–6716. https://doi.org/10.1002/2013JC009067

Griffies, S. M., Winton, M., Anderson, W., Benson, R., Delworth, T. L., Dufour, C. O., et al. (2015). Impacts on ocean heat from transient mesoscale eddies in a hierarchy of climate models. *Journal of Climate*, 28(3), 952–977. https://doi.org/10.1175/JCLI-D-14-00353.1

Iudicone, D., Rodgers, K. B., Plancherel, Y., Aumont, O., Ito, T., Key, R. M., et al. (2016). The formation of the ocean's anthropogenic carbon reservoir. *Scientific Reports*, 6(1), 35473. https://doi.org/10.1038/srep35473

Jackett, D. R., McDougall, T. J., England, M. H., & Hirst, A. C. (2000). Thermal expansion in ocean and coupled general circulation models. *Journal of Climate*, 13(8), 1384–1405. https://doi.org/10.1175/1520-0442(2000)013<1384:TEIOAC>2.0.CO;2

Khatiwala, S., Primeau, F., & Hall, T. (2009). Reconstruction of the history of anthropogenic CO_2 concentrations in the ocean. *Nature*, 462, 246–249.

Khatiwala, S., Tanhua, T., Mikaloff Fletcher, S., Gerber, M., Doney, S. C., Graven, H. D., et al. (2013). Global ocean storage of anthropogenic carbon. *Biogeosciences*, 10(4), 2169–2191. https://doi.org/10.5194/bg-10-2169-2013

Kostov, Y., Armour, K. C., & Marshall, J. (2014). Impact of the Atlantic meridional overturning circulation on ocean heat storage and transient climate change. *Geophysical Research Letters*, 41, 2108–2116. https://doi.org/10.1002/2013GL058998

Marshall, J., & Radko, T. (2003). Residual-mean solutions for the Antarctic circumpolar current and its associated overturning circulation. *Journal of Physical Oceanography*, 33(11), 2341–2354. https://doi.org/10.1175/1520-0485(2003)033<2341:RSFTAC>2.0.CO;2

Marshall, J., & Speer, K. (2012). Closure of the meridional overturning circulation through Southern Ocean upwelling. *Nature Geoscience*, 5(3), 171–180. https://doi.org/10.1038/ngeo1391

Morrison, A. K., Griffies, A. M., Winton, W., Anderson, W. G., & Sarmiento, J. L. (2016). Mechanisms of Southern Ocean heat uptake and transport in a global eddying climate model. *Journal of Climate*, 29(6), 2059–2075. https://doi.org/10.1175/JCLI-D-15-0579.1

Morrison, A. K., & Hogg, A. M. C. (2013). On the relationship between Southern Ocean overturning and ACC transport. *Journal of Physical Oceanography*, *43*(1), 140–148. https://doi.org/10.1175/JPO-D-12-057.1

Morrison, A. K., Hogg, A. M. C., & Ward, M. L. (2011). Sensitivity of the Southern Ocean overturning circulation to surface buoyancy forcing. *Geophysical Research Letters*, *38*, L14602. https://doi.org/10.1029/2011GL048031

Nagelkerken, V., & Connell, S. D. (2015). Global alteration of ocean ecosystem functioning due to increasing human CO_2 emissions. *PNAS*, *112*(43), 13,272–13,277. https://doi.org/10.1073/pnas.1510856112

Poloczanska, E. S., Brown, C. J., Sydeman, W. J., Kiessling, W., Schoeman, D. S., Moore, P. J., et al. (2013). Global imprint of climate change on marine life. *Nature Climate Change*, *3*(10), 919–925. https://doi.org/10.1038/nclimate1958

Riebesell, U., Körtzinger, A., & Oschlies, A. (2009). Sensitivity of marine carbon fluxes to ocean change. *Proceedings of the National Academy of Sciences of the United States of America*, *106*(49), 20,602–20,609. https://doi.org/10.1073/pnas.0813291106

Sabine, C. L., Feely, R. A., Gruber, N., Key, R. M., Lee, K., Bullister, J. L., et al. (2004). The ocean sink for anthropogenic CO_2. *Science*, *305*(5682), 367–371. https://doi.org/10.1126/science.1097403

Winton, M., Griffies, S. M., Samuels, B. L., Sarmiento, J. L., & Frölicher, T. L. (2013). Connecting changing ocean circulation with changing climate. *Journal of Climate*, *26*(7), 2268–2278. https://doi.org/10.1175/JCLI-D-12-00296.1

Wohlers, J., Engel, A., Zöllner, E., Breithaupt, P., Jürgens, K., Hoppe, H., et al. (2009). Changes in biogenic carbon flow in response to sea surface warming. *Proceedings of the National Academy of Sciences*, *106*(17), 7067–7072. https://doi.org/10.1073/pnas.0812743106